ACS APPLIED MATERIALS & INTERFACES

www.acsami.org

Research Article

Donor–Acceptor Conjugated Polyelectrolytes for Organic Electrochemical Transistors: Interplay between Main-Chain Charge Carriers and Side-Chain Ions

Andreas W. Erhardt,* Julian Hungenberg, Linus Hager, Florian Meichsner, Meike Kuhn, Wen Liang Tan, Elena Chulanova, Nigel Kirby, Mukundan Thelakkat, and Christopher R. McNeill

Cite This: *ACS Appl. Mater. Interfaces* 2026, 18, 8493–8506

Read Online

ACCESS | Metrics & More | Article Recommendations | Supporting Information

ABSTRACT: Poly(diketopyrrolopyrrole) (PDPP)-based π-conjugated polyelectrolytes (CPEs), facilitating either electron or hole transport for applications in organic electrochemical transistors (OECTs), were synthesized. By equipping each polymer main-chain with neutral, anionic, or cationic side chains, the resulting series of polymers encompasses all possible combinations of negative, positive, and neutral side-chain ionic charges in combination with in situ-generated holes or electrons on the backbone. This investigation focuses on uncovering intramolecular synergies and antagonisms of the mixed conductors (ions and electrons), with a special emphasis on parameters relevant to both p- and n-type OECT devices using CPEs. While UV–vis absorption spectroscopy suggests only small changes in the optoelectronic properties among the differently charged polymers, in situ and operando GIWAXS analyses revealed significant differences in swelling behavior. We observed that cationic and anionic side chains induce distinct alterations in interlamellar spacing with varying degrees of swelling influenced by electrochemical doping and ion diffusion, which is controlled by the sign of the applied potential. Anionic side chains favor hole transport and enable an earlier oxidation onset of the donor CPE, as demonstrated in the OECT and spectroelectrochemistry (SEC) studies. Such changes are crucial for improving the p-type OECT efficiency and responsiveness. The opposite effect is observed in cationic polyelectrolyte hole conductors. Conversely, electron-transporting materials benefit from cationic side chains, while anionic side chains prove detrimental for n-type device operation. These results suggest a general design strategy for anionic or cationic donor and acceptor materials for the exploitation of OECT applications, where the formation and transport of charge carriers formed in operando (electrons or holes) are favored by the opposite side-chain ions immobilized in a CPE chain, resulting in high drain current at low gate voltages, improved transconductance, and low redox onset voltage.

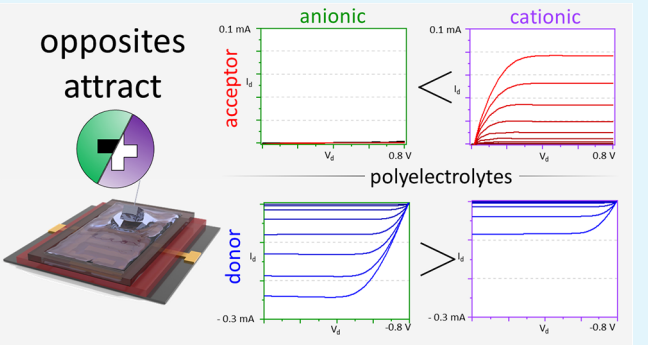

KEYWORDS: *organic electrochemical transistors, conjugated polyelectrolytes, bioelectronics, mixed ionic electronic conductors, operando GIWAXS*

INTRODUCTION

In the field of bioelectronics, biological and electronic signals are interfaced. Such coupling can either be a diagnostic tool, like in an electrocardiogram, during blood sugar measurements, or used to stimulate living tissue, such as in pacemakers.[1] While current devices are applicable in connection with some living tissue, highly sensitive sensing of very soft tissue, like brain matter, is not possible long-term, due to a mismatch in the materials' Young's moduli and consequent scar formation.[2] A promising class of devices that can be based on softer materials and therefore designed to be compatible with softer tissue is organic electrochemical transistors (OECTs). Additionally, they allow access to an increased signal-to-noise ratio during biosensing compared to standard metal electrodes. An OECT consists of source and drain electrodes connected through an electrochemically responsive semiconductor. The redox state of this semiconductor, and thereby its conductivity, is switched by a gate electrode, which is connected to the active layer via an electrolyte. To be switchable through biological stimuli, the active layer needs to partake in a redox reaction at low

Received: October 3, 2025
Revised: January 13, 2026
Accepted: January 20, 2026
Published: January 29, 2026

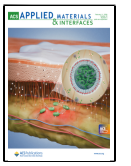

https://doi.org/10.1021/acsami.5c19784
ACS Appl. Mater. Interfaces 2026, 18, 8493–8506

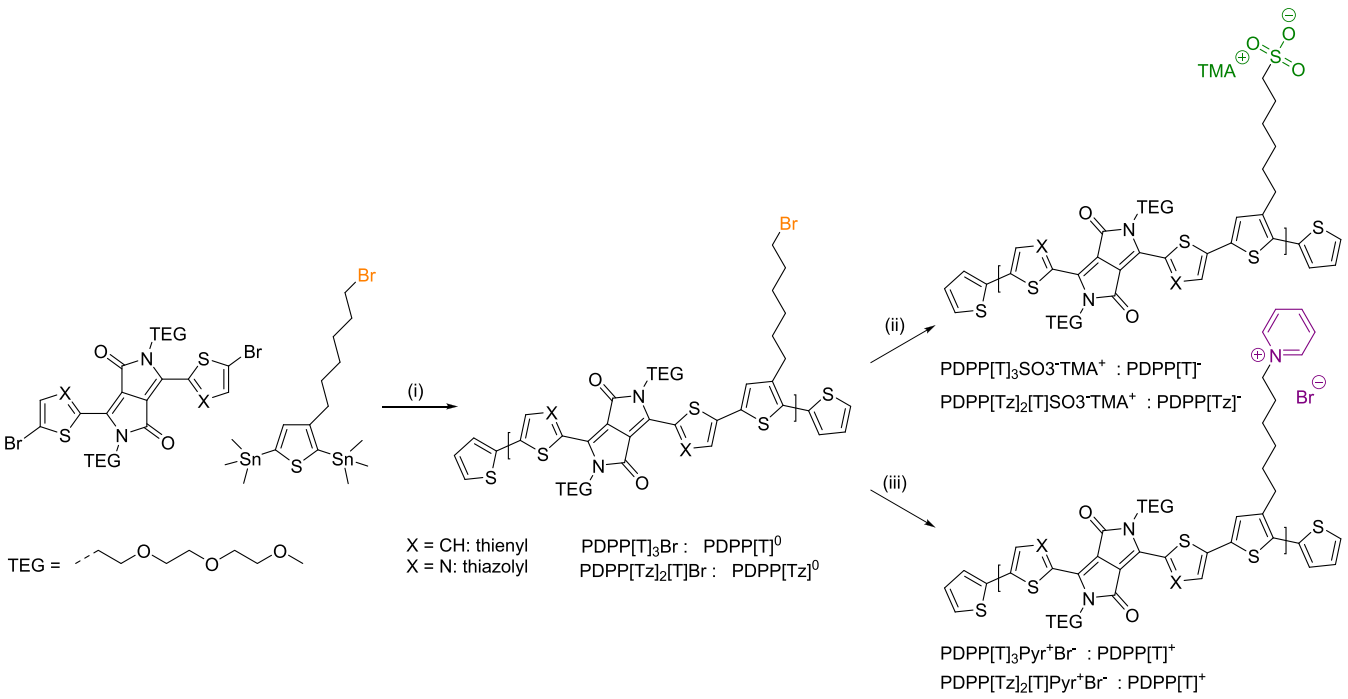

Figure 1. Synthesis pathway yielding a series of four conjugated polyelectrolytes, PDPP[T]$_3$SO$_3^-$TMA$^+$, PDPP[Tz]$_2$[T]SO$_3^-$TMA$^+$, PDPP[T]$_3$Pyr$^+$Br$^-$, and PDPP[Tz]$_2$[T]Pyr$^+$Br$^-$ denoted as PDPP[T]$^-$, PDPP[Tz]$^-$, PDPP[T]$^+$, and PDPP[Tz]$^+$, respectively, starting with the Stille polycondensation of thiophene or thiazole-flanked DPP and a brominated hexylthiophene derivative, yielding two precursor polymers, PDPP[T]$_3$Br and PDPP[Tz]$_2$[T]Br (denoted as PDPP[T]^0 and PDPP[Tz]^0) carrying Br terminal group on the side chain. (i): 1: tri(o-tolyl)phosphine, Tris(dibenzylideneacetone)dipalladium(0), chlorobenzene, 60 min, 180 °C, microwave, 2:2-(tributylstannyl)thiophene, 5 min, 180 °C, microwave, 2-bromothiophene, 5 min, 180 °C, microwave. Subsequently, the brominated side-chain functionalities were substituted with anionic and cationic moieties, yielding the respective polyelectrolytes. (ii): Tetramethylammonium sulfite, 1,2-dichlorobenzene: DMSO (v:v = 6:1), 40 °C, 24 h. (iii): pyridine, chloroform, reflux, 2 d.

potentials to operate in a similar potential regime, e.g., as synapses, and to avoid electrolysis, high bias stress, and power consumption.[3,4] Fortunately, either oxidation or reduction in this potential window below approximately ±1 V is possible for most conjugated polymers, with n-type operation (i.e., electron transport) in relatively electron-deficient acceptor materials and p-type operation (i.e., hole transport) in electron-rich donors.[5] Further, the active layer must be able to accommodate ionic charges to enable volumetric charge compensation, which is necessitated by the injected charge carriers during the redox reaction on the semiconductor molecule, commonly a polymer backbone. Despite the large variety of conjugated polymers under research, e.g., for organic photovoltaic (OPV) research, the majority of those materials are hydrophobic and therefore lack the required compatibility with biologically relevant media and ions. Therefore, modification of such molecular structures is vital to increasing the suitability for OECT-based bioelectronic applications. Commonly, employing the modularity of conjugated polymers, classical hydrophobic side chains can be substituted with polar substituents and, in this way, adapted for application in the field of OECTs. Examples are the polythiophenes P3MEEMT and P3MEEET, derived from P3HT, as well as diketopyrrolopyrrole or naphthalene bisimide-based polymers, with oligoethylene glycol side chains.[5−10,14] Besides oligoethylene glycol side chains, ionic side-chain functionalization is intriguing because synergistic effects between the main and side chains can lead to effects like self-compensation or self-doping.[11,12] Even though the first anionic CPE for p-type devices was reported in 2014, the number of established CPE materials is relatively low, and almost no cationic donor CPE or CPEs for n-type devices have been reported.[11,13] A fundamental question here is how the immobilized side-chain ions interact and influence the charge carriers created in operando in a device such as an OECT working in an aqueous medium. There is a need to understand the interplay of the hole/electron transport in OECTs using CPEs having different ionic charges immobilized at their side chains, even though the most studied OECT materials with high μC^* are based on OEG functionalized organic mixed ion-electron conductors (OMIECs) rather than CPEs.[12] A detailed study of both anionic and cationic CPEs suitable for p- and n-type OECT devices to evaluate their potential is still missing. Also, from a standpoint of studying negatively charged biomolecules, suitable cationic CPEs are of high interest, e.g., the interaction of DNA and cationic CPEs offers a promising approach to DNA-incorporated bioelectronics.[15]

This work covers the systematic synthesis, application, and understanding of donor−acceptor conjugated polyelectrolytes (CPEs) for OECT applications. To comprehend possible intercorrelations between main-chain charge carriers and side-chain ionic charges in these mixed conductors, both donor and acceptor polymers with cationic and anionic side chains are designed and comparatively studied in the dry state and wet state, as well as in operando GIWAXS and OECT devices.

RESULTS AND DISCUSSION

Preliminary Considerations

Historically, a broad understanding of conjugated polymers was obtained based on poly(thiophene) derivatives due to the

https://doi.org/10.1021/acsami.5c19784
ACS Appl. Mater. Interfaces 2026, 18, 8493−8506

Table 1. Molecular Mass Distribution and Thermal Properties of the Synthesized Polymers

polymer	short name	M_n [kg mol^{-1}][a]	$Đ$[a]	$T_{5\%}$ [°C][b]	ambient swelling [wt %][b]
PDPP[T]$_3$SO$_3^-$TMA$^+$	PDPP[T]$^-$	23.9	3.5	286	3.2
PDPP[T]$_3$Br	PDPP[T]^0	22.3	3.5	296	0.4
PDPP[T]$_3$Pyr$^+$Br$^-$	PDPP[T]$^+$	24.0	3.5	225	0.8
PDPP[Tz]$_2$[T]SO$_3^-$TMA$^+$	PDPP[Tz]$^-$	26.5	2.3	263	6.2
PDPP[Tz]$_2$[T]Br	PDPP[Tz]^0	24.7	2.3	295	0.2
PDPP[Tz]$_2$[T]Pyr$^+$Br$^-$	PDPP[Tz]$^+$	26.6	2.3	229	0.8

[a]Determined via SEC ($CHCl_3$, PS calibration) for the neutral polymers PDPP[T]^0 and PDPP[Tz]^0, and calculated for the ionic polymers, assuming that functionalization does not change the degree of polymerization. [b]Extracted from TGA (N_2 atmosphere, 10 K min^{-1}).

high control of molecular weight, tacticity, and end group fidelity during polymerization using Kumada catalyst transfer polymerization.[12,13] While these homopolymers were superseded by a new generation of donor−acceptor polymers for cutting-edge applications in OPV and transistors, the fundamental knowledge that they provide is still valuable.[16,17] This can be illustrated if the thiophene-based anionic polyelectrolyte PTHS$^-$ TMA$^+$ is considered, as it is an early example of OECT active layer materials and is still subject to regular improvements.[11,18] Due to the accessibility of polythiophene derivatives and the high density of (ionic) side-chain functionalization, we chose to investigate the subject of cationic polyelectrolytes, based on the cationic polyelectrolyte P3PyHT$^+$ Br$^-$.[19,20] The advantage of a complementary cationic system to anionic polyelectrolytes is a potentially altered interaction with ionic and biological matter and synergistic fabrication in polyplex systems.[20,21] However, as OECT characterization (Figures S1 and S2) revealed, the investigated cationic polyelectrolytes produce barely working OECT devices, despite no change in the polymer backbone, compared to the more efficient anionic CPE, PTHS$^-$ TMA$^+$.[11,20] An attempt to understand this difference in OECT behavior could be based on the interaction of positive electronic charge carriers (i.e., holes) introduced by the applied gate voltage on polythiophene segments and the tethered positive side-chain Py$^+$ ions.[22] Despite no definite explanation, this observation prompted the question regarding the interplay of charges in a special mixed conductor, such as CPEs, when applied in transistors. Moreover, we ask whether a general guide for interaction between main- and side-chain charges exists and, in extension, if such an effect is also observable in cationic acceptor polyelectrolytes for n-type OECT operation. The assumption that beneficial effects are established in cationic acceptor polymers is supported by a recently reported material by Sommer et al., which reaches extraordinary OECT benchmark values.[23] Unfortunately, a broad and systematic study of cationic and anionic donor and acceptor polyelectrolytes cannot be based on previous systems due to the unipolar character of these materials. Therefore, poly(diketopyrrolopyrrole) (PDPP) copolymers, which can be easily structurally tuned to favor electron, hole, or ambipolar transport, were chosen as a more suitable material class for a comparative study. Here, we seek to understand the interplay of ionic charges with the in situ-generated electronic charge carriers (holes or electrons) in PDPP-based CPEs under working conditions in OECTs.

Material Design and Synthesis

The series of polymers was designed based on the copolymerization of diketopyrrolopyrrole (DPP) derivatives and bromohexylthiophene. This platform consists of two versatile motifs that can be modified to obtain polymers with the desired side-chain charges and the controllable tendency of the polymer to donate or accept electrons.

The electronic character of DPP-based polymers is decisively influenced by the aromatic substituents ("flanking units") of the dilactam core, capable of yielding a range of unipolar donor, acceptor, or ambipolar materials.[24−27] Specifically, polymers incorporating thienyl-linked DPP (Figure 1, X = CH) facilitate hole conduction predominantly, whereas analogous polymers with thiazolyl flanking units (Figure 1, X = N) exhibit a higher affinity to electron transport.[26,28] Therefore, these two polymer backbones were chosen for a comparative study of the respective polyelectrolytes, both cationic and anionic. For this, the side-chain charges can be controlled on the second thiophene-based comonomer. Due to the brominated side-chain functionality, various polymer-analogous nucleophilic substitution reactions are accessible.[13,19,29] The general synthetic scheme is shown in Figure 1. The synthesis of the respective monomers is described in detail in the Supporting Information. In short, the brominated precursor polymers were synthesized via microwave-assisted Stille polycondensation and end-capped with trimethyl(thiophen-2-yl)stannane and 2-bromothiophene to prevent the presence of reactive chain ends. After Soxhlet extraction of short polymer fractions and catalyst residues, polymers with appropriate molecular mass distributions were obtained, as shown based on GPC analysis (Table 1, Figures S3, and S4). The precursor polymers will be termed PDPP[T]^0 and PDPP[Tz]^0, where the flanking unit is denoted by the brackets and the side-chain charge in the superscript.

The anionic CPEs were obtained by dissolving the respective precursor in a mixture of 1,2-dichlorobenzene (*o*-DCB) and dimethyl sulfoxide (DMSO). After complete dissolution, freshly prepared tetramethylammonium sulfite was added and reacted for 24 h at 40 °C, yielding the anionic polyelectrolytes PDPP[T]$^-$ and PDPP[Tz]$^-$. Reaction success was apparent when water/methanol was added to the cooled reaction mixture, which readily dissolved the anionic polyelectrolytes. Salt and DMSO residues were removed via exhaustive dialysis (cutoff 3.5 kDa) vs water/methanol. The cationic polyelectrolytes were synthesized according to the procedure reported by Rubio-Magnieto et al., yielding the polymers PDPP[T]$^+$ and PDPP[Tz]$^+$.[19] ^{1}H NMR spectra were recorded to assess the success of the polymer-analogous reactions (Figures S5 and S6). While the broad signals inherent to polymer NMR make analysis based on signal area impossible, full conversion is indicated by several spectral changes: Proton signals, characteristic of the side-chain protons, in α- and β-positions to the bromo substituent at δ = 3.5 and δ = 2.7 ppm shift completely during the reaction.[29] Instead, new aromatic signals can be found in PDPP[T]$^+$ and PDPP[Tz]+, corresponding to pyridinium substituents. PDPP-

https://doi.org/10.1021/acsami.5c19784
ACS Appl. Mater. Interfaces 2026, 18, 8493−8506

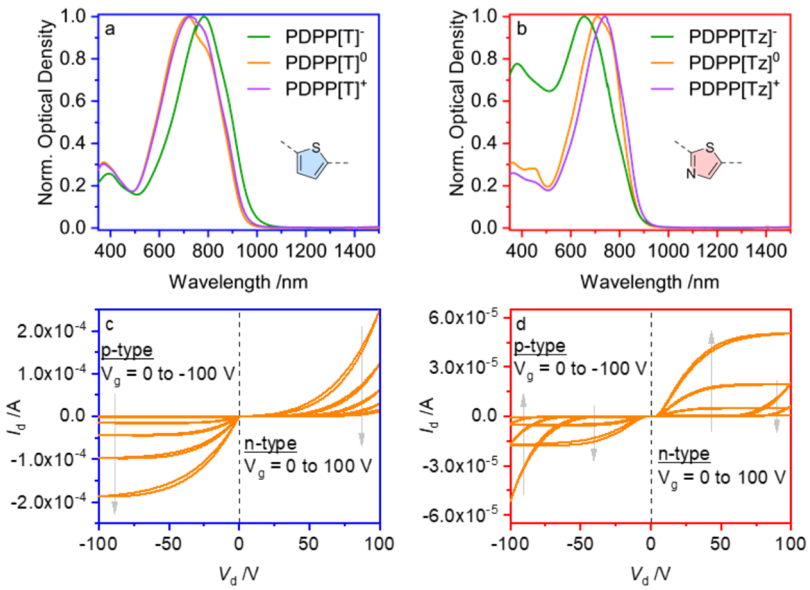

Figure 2. UV−vis absorption spectra of the series of thiophene- (a) and thiazole-linked (b) polymers dissolved in good solvents ($CHCl_3$ for neutral polymers, MeOH for anionic polyelectrolytes, and MeOH: $CHCl_3$ (vol: vol = 1:1), c = 0.2 g L^{-1}). OFET output characteristics of the nonionic polymers PDPP[T]^0 (c) and PDPP[Tz]^0 (d). The transistors were used in the p-type regime (V_g and $V_d \leq 0$ V) and n-type regime (V_g and $V_d \geq 0$ V), revealing unipolar hole transport for PDPP[T]^0 and predominant electron transport in PDPP[Tz]^0.

[T]$^-$ and PDPP[Tz]$^-$ do not show any interpretable NMR signal beyond the tetramethylammonium peak at δ = 3.2 ppm, which agrees with the NMR analysis of similar anionic polyelectrolytes.[12]

Overall, six conjugated polymers, among them four CPEs, were obtained with properties summarized in Table 1. The respective measurements (GPC, TGA) are included in Figures S3−S7. The materials are thermally stable up to at least 225 °C ($T_{5\%}$). Therefore, the maximum annealing temperature for the following studies was 200 °C to exclude thermal degradation. An initial weight loss step can be attributed to the loss of water, which is taken up from ambient moisture (i.e., air humidity). This is accounted for when the $T_{5\%}$ temperatures are determined. The degree of ambient swelling, visible in the thermogravigrams, is the first indication of different affinities of the polymers toward water. As listed in Table 1, the anionic CPEs PDPP[T]$^-$ and PDPP[Tz]$^-$ take up a higher amount of ambient moisture than the cationic CPEs PDPP[T]$^+$ and PDPP[Tz]$^+$, which in turn exhibit higher degrees of swelling than the neutral materials.

Ex-Situ Analysis

UV−Vis Absorption. The extent of the impact of side chain substitution on the optoelectronic properties was investigated first, based on UV−vis spectroscopy in solution for all of the polymers (Figure S8). In the solution spectra of the series with thiophene as the flanking unit (PDPP[T]$^-$, PDPP[T]^0, and PDPP[T]$^+$, Figure 2a,b), the anionic CPE, PDPP[T]$^-$, shows slightly red-shifted λ_{max} values compared to the other two polymers. Similarly, among the thiazole-containing polymers, PDPP[Tz]$^-$ PDPP[Tz]^0 and PDPP-[Tz]$^+$, the anionic PDPP[Tz]$^-$ shows a slight hypsochromic shift in absorption compared to the other two polymers. The reason why the anionic CPEs show this change compared to their neutral species is not trivial to explain, since parameters which influence the planarity of the chain and aggregation even in good solvents, e.g., the effect of the size of the side-chain ion, polarity of the different solvents used, can have combined effects. In general, changes in the side-chain functionalities only slightly change the absorption properties in good solvents, likely caused by a changed mode and degree of aggregation.

The absorption of polymer thin films reveals that absorption properties are not influenced by the side-chain modification for the donor polymers containing thiophene moieties, whereas in the series of thiazole-containing polymers, PDPP[Tz]− shows a hypsochromic shift compared to the neutral and cationic polymers again. This applies to pristine as well as annealed polymer films.

OFET Charge Transport Properties. Before meaningful correlations between main-chain charge carriers and side-chain ionic charges can be established, the charge carrier properties regarding the donor and acceptor behavior of the polymers in their neutral states (PDPP[T]^0 and PDPP[Tz]^0), as well as CPEs, must be verified. A suitable method is characterization via organic field-effect transistors, which reveal charge carrier mobility, threshold voltage, and majority charge carrier (electron or hole). Therefore, bottom-gate bottom-electrode transistor devices were prepared using the two neutral polymers, and output as well as transfer characteristics were measured for both the gate and drain voltage ranges of −100 to +100 V.

The p- and n-type output characteristics of the neutral polymers PDPP[T]^0 and PDPP[Tz]^0 are displayed in Figure 2c,d, respectively. The comparison reveals that the thiophene-containing polymer is a unipolar hole conductor with an electron mobility of μ_h = 1.2 × 10^{-2} cm^2 V^{-1} s^{-1} and a threshold voltage of $V_{th\text{-}h}$ = −33 V. In contrast, the thiazole-flanked PDPP[Tz]^0 is an ambipolar semiconductor with electrons as the majority charge carriers. For PDPP[Tz]^0, charge carrier mobilities of μ_e = 7.8 × 10^{-3} cm^2 V^{-1} s^{-1} and μ_h = 4.0 × 10^{-3} cm^2 V^{-1} s^{-1}, as well as threshold voltages of $V_{th\text{-}e}$ = +53 V and $V_{th\text{-}h}$ = −61 V, were determined after thermal annealing of the device at 150 °C, for 15 min, in a N_2 atmosphere. The hole contribution to electronic transport does not hinder the investigation of interactions between side-chain

https://doi.org/10.1021/acsami.5c19784
ACS Appl. Mater. Interfaces 2026, 18, 8493−8506

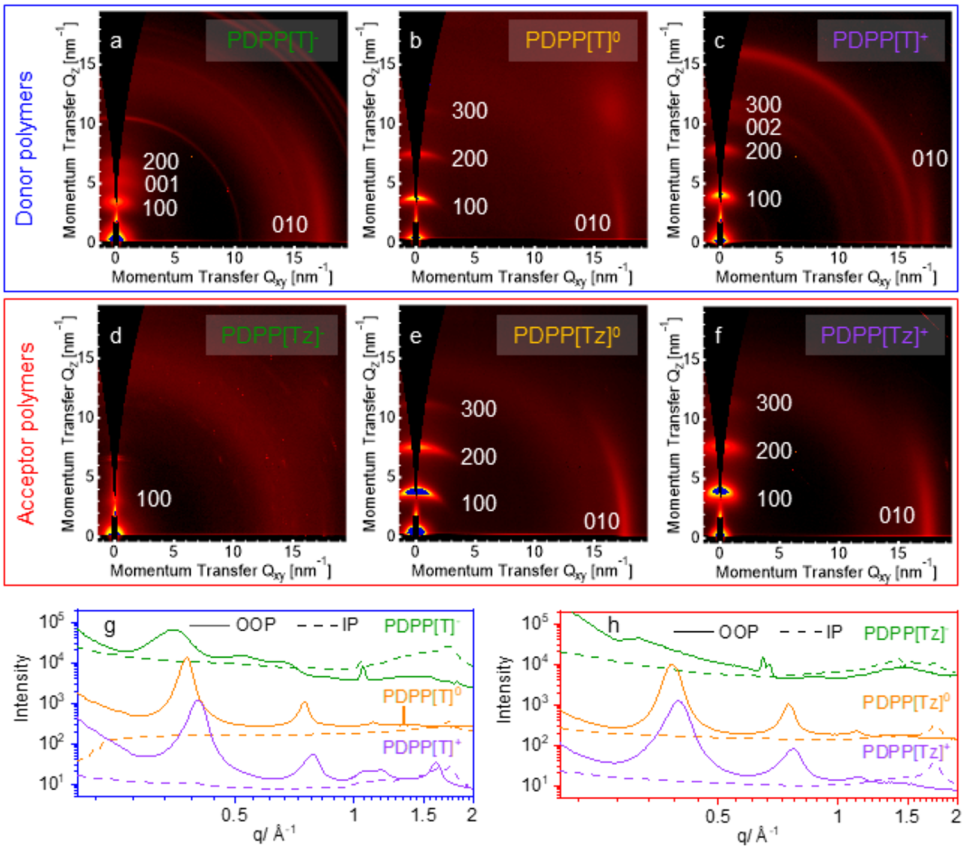

Figure 3. Dry state GIWAXS patterns were recorded in vacuo close to the critical incident angle after annealing for 15 min at 200 °C. Panels (a–c) show the 2D GIWAXS data for the thiophene-based materials, and panels (d–f) show the 2D GIWAXS data for the thiazole polymers. The respective horizontal and vertical line profiles are included to elucidate the different unit cell spacings (g, h).

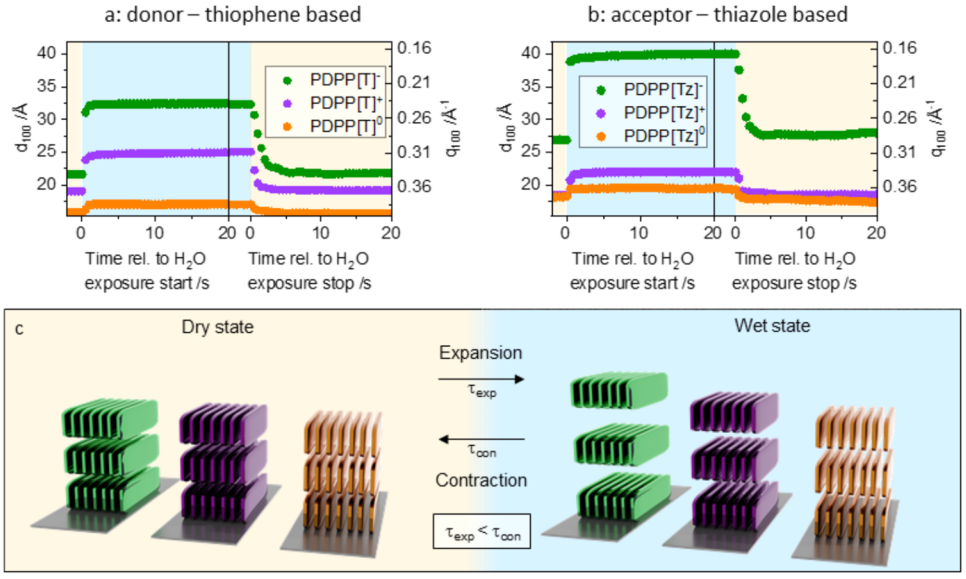

Figure 4. 100 lamellar spacing of the thiophene- (a) and thiazole (b)-based polymers as a function of time during dynamic swelling experiments. The time scale axis is plotted relative to the exposure of the films to water vapor. A stronger extent of swelling for the anionic polymers, compared to the cationic ones, can be observed, with the smallest change in 100 spacing in neutral materials (c). For all materials, the swelling process is faster than deswelling, as revealed by fitting with an exponential decay function.

charges and main-chain charges formed at an applied gate potential. This is further supported by the fact that the employed bottom-gate bottom gold-contact OFET architecture typically underestimates n-type properties.[30]

Despite no structural change in the polymer backbone, the conversion from neutral conjugated polymers to anionic polyelectrolytes decreases the charge carrier mobility in both systems, PDPP[T]$^-$ and PDPP[Tz]$^-$ (cf. Figure S9). The

https://doi.org/10.1021/acsami.5c19784
ACS Appl. Mater. Interfaces 2026, 18, 8493–8506

reason for this can lie in a change in crystallinity and/or morphology arising out of distorted structure formation, caused by the bulky ionic groups or the introduction of trap sites. Interestingly, the inclusion of anionic side chains fully suppresses electron transport in PDPP[Tz]$^-$, resulting in unipolar hole conduction. This is in accordance with our preliminary observation for cationic polythiophene, where we assumed hindered charge transport based on the identical sign of electronic charge carriers and tethered cationic side-chain ions.[20] Ionic contributions to the drain current seem to obscure the electronic charge transport in p-type devices for the two cationic polyelectrolytes PDPP[T]$^+$ and PDPP[Tz]$^+$, obscuring the impact of cationic moieties on the OFET electron mobility, as apparent in Figure S9c,d. The OFET transfer characteristics of all polymers are listed in Table S1. No values were extracted for the cationic polymers due to the aforementioned ionic charge transport contributions.

Thin-Film Structure in the Dry State. The optoelectronic properties of conjugated polymers and CPEs in devices strongly depend on the thin-film morphology. In the discussed case, anisotropy in the thin-film crystalline structure leads to anisotropy of the charge transport properties.[26,31] Therefore, the polymer nanostructure was investigated based on grazing-incidence wide-angle X-ray scattering (GIWAXS).

Figure 3a−c displays the 2D scattering patterns of the thiophene-based donor polymers after annealing at 200 °C for 15 min. The respective thiazole-based acceptor counterparts, which were subjected to the identical thermal treatment protocol, are included in Figure 3d,e. The *h*00 peaks of all polymers are located on the Q_z axis of the scattering patterns, with a discernible 010 signal in the Q_{xy} direction. This is indicative of edge-on-oriented crystallites, where the polymer chains are oriented parallel to the surface with the side chains orthogonal to the substrate, as sketched later in Figure 4. Solely based on the mode of surface-relative crystallite orientation ("texture"), no significant difference in charge transport properties is expected. Quantitative insights into the crystallite orientation were obtained by analyzing the intensity of the 100 reflexes as a function of the sin(χ)-corrected polar angle χ (Figure S10). From the signal area in the intervals 5−45, 45−85°, and the area of the isotropic population, the texture contents were inferred (Figure S11). In all cases, a predominantly nonoriented structure is formed directly after coating, with edge-on contents varying between 23 and 45% and face-on contents below 4% in all cases. During annealing, a trend of increasing orientation is pronounced for neutral and cationic polyelectrolytes, which is expected to lead to more efficient in-plane charge transport.

In addition to the pronounced lamellar order, the two thiophene-linked polyelectrolytes PDDP[T]$^-$ and PDPP[T]$^+$ exhibit a reflex of the 00l series, indicating a relatively high order in the direction of the polymer main chain. For a more thorough analysis, the in-plane and out-of-plane scattering profiles were extracted from the 2D patterns. The respective patterns in Figure 3g,h reveal a significantly decreased scattering intensity in the anionic polyelectrolytes, compared to the remaining materials. This is caused by a qualitatively lower degree of crystallinity, attributed to the distortion of the polymer microstructure by the bulky sulfonate and tetramethylammonium groups. In contrast, the smaller brominated and planar pyridinium bromide end-groups can be incorporated into the polymer structure with less disruption. The low order causes the reduced charge transport efficiency observed in the OFET studies. This effect is supported by an increased interlamellar spacing, as indicated by the low 100 *Q*-position (cf. Tables S2 and S3). When subjected to thermal annealing, the materials exhibit pronounced structural consolidation, evidenced by a significant reduction in the 100 spacing after treatment at 100 and 200 °C (Figures S12−S15). This effect is most pronounced for the cationic polyelectrolytes, which display relatively large 100 spacings in the as-cast state. Upon annealing at 200 °C, lamellar contraction is substantially stronger than in the other polymers, resulting in the cationic materials exhibiting the lowest lamellar spacing after thermal treatment. This hints at reorganization and tighter packing of the cationic polyelectrolytes at high temperatures. Overall, the thin-film morphology of the neutral and cationic polymers is similar, while the anionic polyelectrolytes form mostly amorphous films. This is also reflected by the increased peak width (full width at half-maximum, fwhm) of the anionic materials, which is inversely proportional to the crystallite coherence length. Any influence of ambient moisture can be ruled out because the polymer films were stored under ultrahigh vacuum before and during data acquisition.

To access complementary real-space data, the sample topology was investigated by using atomic force microscopy (AFM). Accurate surface information is vital to assess materials for OECT operation, because microporosity can enhance the device transconductance.[32] To evaluate the inherent polymer properties, effects caused by processing must be taken into account. AFM height profiles (Figures S16 and S17) reveal the absence of porosity on the probed length scale in all materials. Furthermore, the surface roughness (root-mean-square, RMS) of the polymers ranges from 0.3 to 2.5 nm, with no discernible trend among the materials. Quantitative PeakForce nanomechanical mapping was employed to obtain spatially resolved mechanical parameters, such as adhesion, indentation, and stiffness of the material. Figure S18 shows that the thiophene-based materials exhibit a stiffness higher than that of their thiazole counterparts, which also leads to a lower indentation. Further, the anionic polyelectrolytes PDPP[T]$^-$ and PDPP-[Tz]$^-$ exhibit a stiffness higher than that of the respective neutral and cationic CPE materials. This agrees well with the available literature, which reports higher Young's moduli for ionic materials like PBFDO or PEDOT: PSS than for neutral polymers like P($g_4$2T-T) or P3HT, measured via nanoindentation[33]

Passive Swelling and Lamellar Expansion under Wet Conditions. OECT materials are designed to interact with (aqueous) electrolytes. In general, high compatibility with the aqueous media usually results in swelling, and low compatibility leads to less swelling. It also affects the charge compensation and storage of ions in the whole film, manifested in the measured volumetric capacitance C^*. Conversely, extensive swelling can lead to a disrupted polymer nanostructure and therefore be detrimental to charge carrier mobility under working conditions, μ_{OECT}.[34] Therefore, knowledge of the structural changes as a result of the interaction of the OECT channel materials with the respective electrolyte systems is beneficial for a fundamental understanding.

Here, as a first step, we focus on the passive swelling under aqueous conditions by characterization via time- and potential-resolved GIWAXS, as it gives access to the selective analysis of the changes in crystalline domains. The annealed materials were subjected to saturated water vapor during continuous GIWAXS image acquisition with a time resolution of 500 ms

https://doi.org/10.1021/acsami.5c19784
ACS Appl. Mater. Interfaces 2026, 18, 8493−8506

to compare the passive swelling behavior of the six polymers. This method only approximates the interaction of the materials with a water droplet or film. Due to the identical measurement conditions, the interaction with water remains directly comparable, ensuring unobstructed GIWAXS pattern analysis without disruptive background interference. This methodology preserves data clarity and facilitates kinetic studies, enabling a deeper understanding of dynamic structural evolution under swelling. A detailed description of the measurement setup and sample preparation is included in Figures S19–S25.

When subjected to water vapor, variations in the *h*00 and 010 peak positions can indicate changes in the interlamellar side-chain or backbone spacing, respectively. A smaller *Q*-value corresponds to the expansion of the crystallite unit cell in the respective direction, indicating swelling, whereas a larger *Q*-value indicates unit cell contraction. Accordingly, Figures S20 and S21 show that all polymers exhibit structural changes when brought in contact with the saturated water vapor. As dynamic measurements were started under ambient conditions, the two anionic polyelectrolytes PDPP[T]$^-$ and PDPP[Tz]$^-$ are already influenced by the ambient moisture, as a comparison to the ex-situ data (Figure 3) reveals. The *Q*-values of the neutral and cationic polymers show no notable difference when samples measured in vacuo and in air are compared. Via radial integration and peak-fitting, the swelling process was quantified in a time-resolved manner, as shown in Figure 4a,b for the time-resolved lamellar distance, extracted from the 100 peak positions. As the $\pi-\pi$ distance remains relatively steady during passive swelling (cf. Figures S24 and S25), the following analysis is focused on the expansion and contraction of the side-chain lamellae. Strikingly, the order of the water affinity, initially observed in TGA measurements, is reflected in GIWAXS analysis. Neutral polymers swell significantly less than the cationic CPEs, which in turn exhibit a smaller lamellar expansion than their anionic counterparts (cf. Figure 4c). This trend is observed in both donor and acceptor polymers. However, by comparison of both systems, the anionic donor shows a higher lamellar expansion than its acceptor counterpart. In contrast, the cationic acceptor polymer swells to a higher extent than does the respective donor polymer.

Fitting the swelling and deswelling processes yields the time constant τ_{exp} of the lamellar expansion and τ_{con} during the contraction (cf. Figures S22, S23, and Table 2). In all cases, the swelling kinetics are faster than the deswelling (contraction) kinetics ($\tau_{exp} < \tau_{con}$).

Table 2. Extent of Lamellar Expansion during Water Vapor-Driven Swelling of the Conjugated Polymers and Time Constants of the Expansion and Contraction Process, Extracted from GIWAXS 100 Signals

material	lamellar expansion [Å][a]	lamellar expansion [%][a]	$\tau_{swelling}$ [s][b]	$\tau_{deswelling}$ [s][b]
PDPP[T]$^-$	7.76	41.8	0.23	1.66
PDPP[T]^0	0.50	3.1	0.26	0.66
PDPP[T]$^+$	2.62	15.2	0.68	1.17
PDPP[Tz]$^-$	14.98	67.5	0.16	1.16
PDPP[Tz]^0	0.78	4.7	0.45	0.74
PDPP[Tz]$^+$	1.66	9.8	0.16	0.55

[a]Absolute and relative difference of the lamellar spacing in the dry and swollen state, each determined by fitting the plateau with constant functions ($y = c$). [b]Extracted by fitting the swelling and deswelling process with exponential decay functions ($y = A\ e^{-t/\tau} + y_0$).

Operando Conditions

Electrochemical gating studies were conducted with aqueous solutions of 0.1 M KCl. This electrolyte offers monovalent salts, providing highly mobile ions that do not engage in strong specific interactions with the polymer. For polyelectrolytes, the essential features of ion uptake, swelling, and charge compensation are governed primarily by the need to balance charge rather than specific reactions of the individual ions. We therefore expect the qualitative trends observed with KCl to be valid for other monovalent electrolytes of similar hydration and mobility. Although minor quantitative differences in kinetics or hydration may arise among K^+, Na^+, Li^+, or their corresponding halides, the underlying mechanism of ion uptake and volumetric response is expected to remain the same. Moreover, KCl is widely used in bioelectronic and OECT research, providing a relevant and standardized electrolyte that reflects physiologically representative ionic environments.

Spectroelectrochemistry (SEC) in Aqueous Medium. During OECT operation of accumulation mode materials (i.e., a priori undoped materials), the polymer partakes in a redox reaction, which converts the material to its conductive state by electrochemical charge injection. This process of (electro)-chemical oxidation and reduction is normally accompanied by electrochromism of the polymer. The ground-state absorption is bleached, and a new feature emerges. This new spectral component is ascribed to polaronic species, i.e., radical anions or cations, responsible for the increased conductivity in operando. The extent of the spectral changes can be qualitatively correlated to the extent of the respective redox reaction. Therefore, spectroelectrochemistry (potential-resolved UV–vis spectroscopy, SEC) in an electrolyte medium is a suitable tool for investigating redox processes.[7,9] Due to the intercorrelation with the processes in the OECT operation using the same electrolyte, SEC also reveals first information about the applicability of the conjugated polyelectrolyte as an active layer material. SEC was conducted with thin films of the polymers on indium-doped tin oxide (ITO) as the working electrode in a three-electrode setup with Ag/AgCl reference and Pt-counter electrodes. The films were gated via a 0.1 M aqueous KCl solution. The spectral changes of the polymers are measured as a function of applied bias and are compiled in Figure 5. SEC measurements under oxidative (V = 0 to 0.8 V) conditions are shown for the donor materials. For the acceptor materials, the spectra were recorded with increasing reductive potentials (0 to −0.8 V).

As showcased in Figure 5a,c,e, all of the thiophene-based polymers are readily oxidized by applying a positive potential. The ground-state absorption ($\lambda_{max} \sim 760$ nm) is bleached, accompanied by the concomitant rise of polaron absorption above 900 nm. The conversion of the neutral to the radical cation species occurs without side reactions, as signified by the clear isosbestic points. When the three spectra of the anionic, neutral, and cation donor polymers are compared, differences in the oxidation onset voltage and extent of conversion are apparent. While the spectrum of PDPP[T]$^+$ at 0.8 V consists of both signatures of the neutral state and polaron peaks, PDPP[T]$^-$ seems to consist only of the featureless signal of the radical cation. The spectra of the acceptor polymers in Figure 5b,d,f show similar behavior, with the ground-state bleach generally being less pronounced and having a lower maximum polaron peak intensity compared to the donor polymers. Strikingly, the anionic acceptor polyelectrolyte

https://doi.org/10.1021/acsami.5c19784
ACS Appl. Mater. Interfaces 2026, 18, 8493–8506

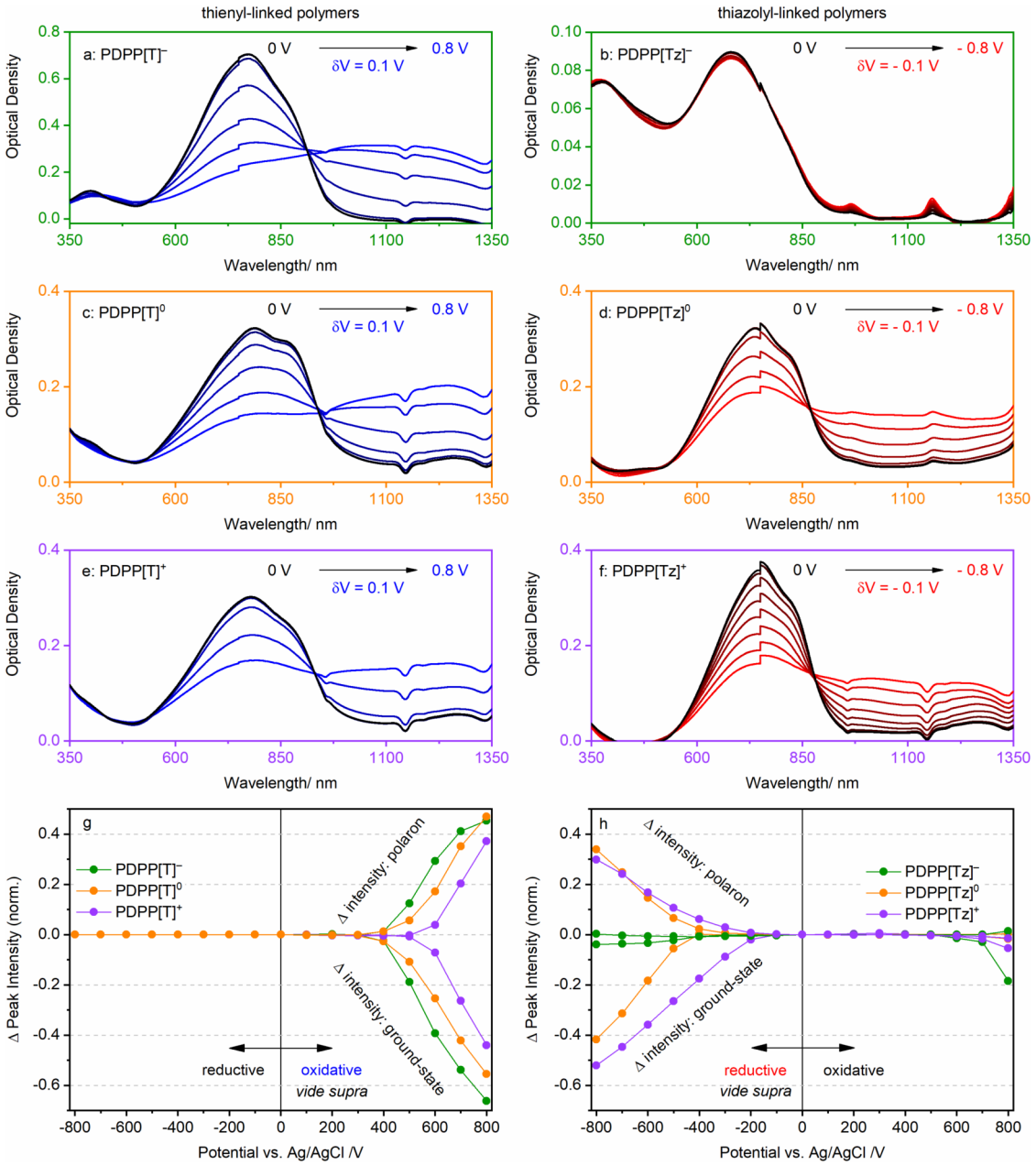

Figure 5. UV−vis-NIR spectroelectrochemistry analysis of the conjugated polyelectrolytes in thin-films on ITO in 0.1 M KCl (aq) medium against the Ag/AgCl reference electrode. For polymers containing thiophene-flanked DPP, the spectra under oxidative conditions are shown (a, c, and e). For the thiazole-containing materials, the spectra under reductive conditions (b, d, and f) are given. For all spectra, the absorption of an uncoated substrate in the electrolyte-filled measurement cell without applied bias was subtracted as background, causing the artifacts at 1140 and 1330 nm. The peak intensity changes of the main- (at 760 nm) and polaron absorption (1200 nm) are shown, normalized to the intensity of the undoped main absorption peak (g and h).

PDPP[Tz]$^-$ does not exhibit a reduction behavior up to −0.8 V.

For in-depth comparison, the absorption intensity of the polymers was normalized to the maximum intensity of the polymer at a potential of 0 V ($I_{\text{normalized}} = I/I_{0\ \text{V-max}}$). To visualize this difference further, the relative peak intensity of the ground state (λ = 760 nm) and polaron signal (λ = 1200 nm) is plotted in Figure 5g for the thiophene-based polymers and Figure 5h for the thiazole-based polymers. From the slopes of the polaron absorption increase or the reduction of the ground-state absorption peak, it can be inferred that the anionic side chains favor a fast oxidation compared to the neutral polymer. The cationic polyelectrolyte, in contrast, exhibits an increased oxidation onset. However, this trend is inverted in the series of acceptor polymers, where cationic moieties cause a decreased reduction onset. Anionic side chains either increase the onset above the investigated potential range or generally prevent the reduction of the acceptor polymer.

OECT Operation. SEC studies indicate that the switching of the redox state via a gating electrolyte is possible. Therefore, the series of polymers should be suitable for application in OECTs, with the exception of PDPP[Tz]$^-$. Based on the previous results, an influence of the side-chain charge on the

https://doi.org/10.1021/acsami.5c19784
ACS Appl. Mater. Interfaces 2026, 18, 8493−8506

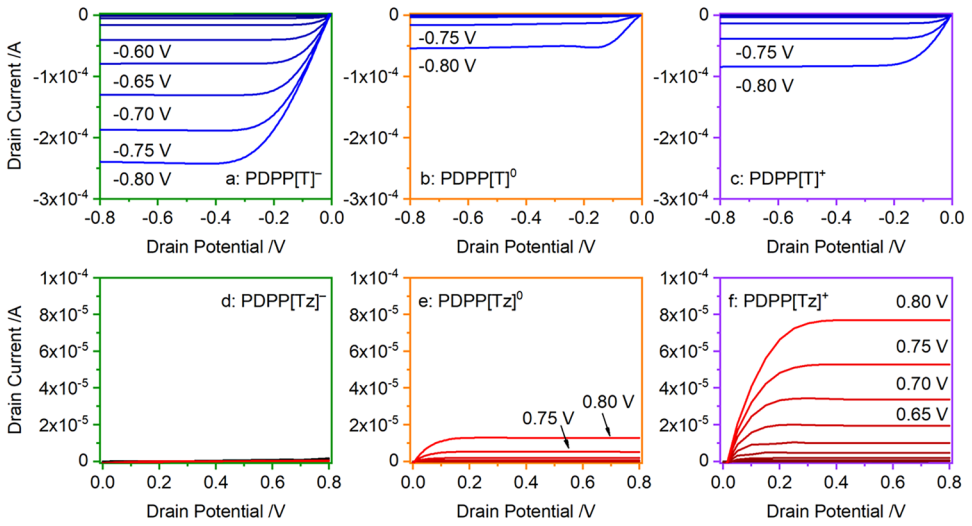

Figure 6. OECT output characteristics for the p-type devices of thiophene-based polymers PDPP[T]$^-$ (a), PDPP[T]^0 (b), and PDPP[T]$^+$ (c) in the accumulation regime (negative gate and drain potential) and for the n-type devices for thiazole-based polymers PDPP[Tz]$^-$ (d), PDPP[Tz]^0 (e), and PDPP[Tz]$^+$ (f) in the accumulation regime (positive gate and drain potentials) against Ag/AgCl.

Table 3. OECT Characteristics of the Investigated Conjugated Polymers[a]

	PDPP[T]$^-$	PDPP[T]^0	PDPP[T]$^+$	PDPP[Tz]$^-$	PDPP[Tz]^0	PDPP[Tz]$^+$
V_{th}/mV	−445	−437	−619		561	455
I_d^{sat}/A @ $\lvert V_g\rvert$ = 0.6 V[b]	-4.0×10^{-5}	-2.2×10^{-7}	-5.5×10^{-7}	1.5×10^{-7}	1.1×10^{-7}	1.0×10^{-5}
$\mu CC^*/F$ cm^{-1} V^{-1} s^{-1}	9.0	0.0	10.7		0.8	5.2
operation	p-type				n-type	

[a]Thiophene-based materials were operated in the p-type accumulation mode, and thiazole-based polymers in the n-type accumulation mode. [b]Absolute saturation drain current at a gate voltage of +0.6 V for n-type operation and −0.6 V for p-type operation, extracted from the output curves at the maximum absolute gate potential.

device operation is to be expected. Hence, the polymers were applied as OECT active layer materials, gated with a Ag/AgCl gate pseudoreference electrode. The polymers were thermally annealed for 15 min at 150 °C, which is well below the thermal degradation onset and above the mass loss step associated with water expulsion. Devices were gated with 0.1 M KCl, aq, under conditions similar to SEC studies.

The OECT output curves for p-type devices in the accumulation mode operation regime for PDPP[T]$^-$ (a), PDPP[T]^0 (c), and PDPP[T]$^+$ (e), and for the n-type devices, also in accumulation mode operation mode for PDPP[Tz]$^-$ (b), PDPP[Tz]^0 (d), and PDPP[Tz]$^+$ (f) are shown in Figure 6. The respective transfer data are included in Figures S26 and S27, with the extracted device parameters given in Table 3. As expected, all polymers except PDPP[Tz]$^-$ provide working devices, either under p-type conditions in the case of thiophene-flanked PDPPs or in the n-type regime, in the case of thiazole-based polymers. This behavior mirrors the findings of SEC studies, where PDPP[Tz]$^-$ was neither oxidizable nor reducible in the tested potential range of −0.8 to +0.8 V. In the series with thiophene as the flanking unit, the incorporation of anionic side chains in PDPP[T]$^-$ leads to improved OECT characteristics, compared to the neutral analog PDPP[T]^0, which is manifested by an increased transconductance, μC^*, high drain current, and earlier current onset. Similar onset values of PDPP[T]$^-$ and PDPP[T]^0 are observed, which is also in accordance with the SEC studies (Figure S26). Cationic side chains on the donor polymer PDPP[T]$^+$ increase the threshold voltage and lower the drain currents, in line with the observations in SEC studies. The trends and OECT parameters are in good accordance with our initial observation concerning anionic and cationic polythiophene derivatives in OFET devices, as both polymer classes exhibit unipolar p-type behavior.

When the series of acceptor polymers PDPP[Tz]$^-$, PDPP[Tz]^0, and PDPP[Tz]$^+$ are considered, a drastic contrast to the observed behavior in the donor materials is apparent. Here, anionic side chains do not improve the operation of the OECT but are detrimental to a transistor device. Here, however, the incorporation of cationic side chains in the CPE PDPP[Tz]$^+$ leads to a notable increase of μC^* and a decrease in the threshold voltage compared to the neutral polymer. Thus, a general observation can be deduced for the studied CPEs from the OECT results that the charge carrier on the main chain (electron or hole) is highly favored by the opposite ionic charge on the side chain. In other words, an anionic CPE as donor (e.g., PDPP[Tz]$^-$) and a cationic CPE as an acceptor (e.g., PDPP[Tz]$^+$) improve the OECT characteristics considerably, compared to their neutral counterparts. On the other hand, OECT characteristics are detrimentally impacted if the charges on the CPEs are reversed, as observed for the polymers PDPP[T]$^+$ and PDPP[Tz]$^-$. One can argue that in an anionic donor CPE, the degree of hole injection and hole transport is strongly favored by the presence of immobilized anions (on the side chain) and mobile TMA$^+$ cations already present in the film. The observed synergy may be due to fast and facile charge self-compensation in the oxidized state via side-chain anions (at applied gate bias) in an anionic donor CPE like PDPP[Tz]$^-$ and in the reduced state via side-chain cations in a cationic acceptor like CPE PDPP[Tz]$^+$. When the side-chain

https://doi.org/10.1021/acsami.5c19784
ACS Appl. Mater. Interfaces 2026, 18, 8493−8506

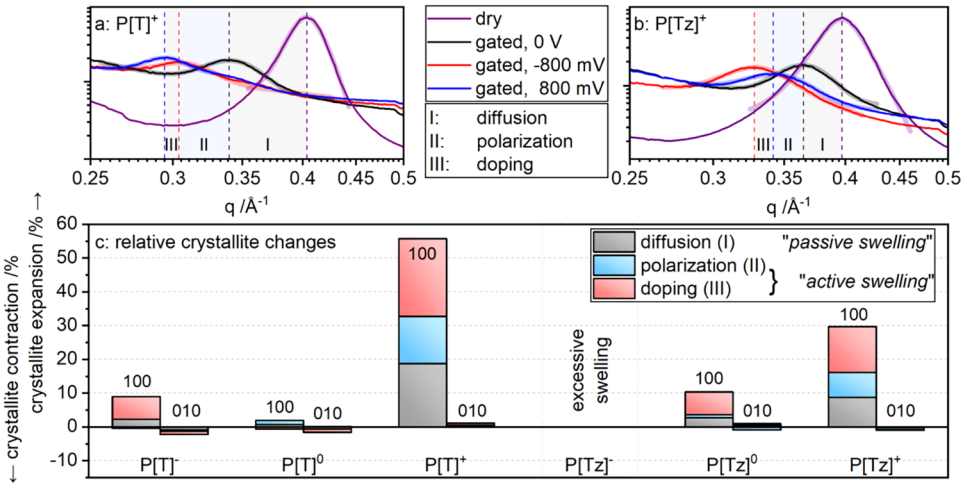

Figure 7. Structural variations of the polymers under different stimuli (in vacuo, immersed in an electrolyte, and gated with ±800 mV). The changes are most notable in the magnification of the 100 reflex region for PDPP[T]$^+$ (a) and PDPP[Tz]$^+$ (b). From the differences in lamellar expansions, three regimes were inferred. (I): diffusion/active swelling, (II): polarization without redox reaction, and (III): doping. The changes in 100 and 010 spacing are compiled for all materials in (c). Scattering profiles are vertically offset for clarity.

charges are reversed, as in PDPP[T]$^+$ and PDPP[Tz]$^-$, this favorable interaction is absent and may hinder the charge generation and transport in such systems. In order to emphasize these effects, one can compare the saturation drain current at a specific applied gate bias (e.g., $|V_g|$ = 0.6 V, see Table 3), where both PDPP[T]$^-$ and PDPP[Tz]$^+$ outperform their counterparts.

For deeper insight, the volumetric capacitance C^* of the polyelectrolytes was determined as a function of the applied potential via electrochemical impedance spectroscopy (EIS) using 0.1 M KCl (aq) as the electrolyte. At low potentials, the donor polymers PDPP[T]$^-$ and PDPP[T]$^+$ (Figure S28) exhibit a low volumetric capacitance of about 0.1 F cm^{-3}, which increases at higher potentials due to the oxidation of the polymers. Consistent with previous observations, the oxidation onset in EIS is at a lower potential for PDPP[T]$^-$, compared to that of PDPP[T]$^+$. Further, the volumetric capacitance of 80.4 F cm^{-3} at 0.75 V is higher for the donor anion, compared to its cationic counterpart, which reaches 31.1 F cm^{-3} at the same voltage. This difference is reflected in the threshold voltage and maximum transconductance of the OECT devices. To put the C^* values, reached with these polyelectrolytes, into context, a previous report of PDPP[T] with triethylene glycol substituents on the thiophene moiety exhibited a volumetric capacitance of 250 F cm^{-3} at 0.75 V, and consistently reached a considerably higher μC^* of 45.[9]

These trends can be qualitatively observed in the EIS data of the acceptor polymers in Figure S29, where a higher C^* is reached by PDPP[Tz]$^+$, compared to that by PDPP[Tz]$^-$. However, the C^* of both acceptor polymers reaches a plateau early on, possibly caused by material degradation in situ.

Active Swelling Studies Using GIWAXS. To clarify the correlation between the OECT and SEC operation, potential-resolved GIWAXS was conducted to investigate active swelling in polymer films under applied potentials of 0 V and ±800 mV in contact with an aqueous electrolyte. An in situ setup was used to monitor changes in the (100) and (010) scattering peaks during electrochemical doping. We adapted the rolling drop method developed by Richter et al. (cf. Figure S30) into a configuration tailored for OECT devices. This modification extends the technique to polyelectrolyte and acceptor materials, enabling operando insights into swelling-induced microstructural changes under realistic device conditions.

The polymer films were annealed at 200 °C for 15 min in air to enhance structural definition and water stability without requiring cross-linking agents. However, for PDPP[Tz]$^-$, either the extensive loss of order led to a decrease of the scattering intensity below detectability, or swelling shifted the (100) peak into the beam stop region, obscuring the signal and preventing its inclusion in subsequent analysis. Interestingly, the lamellar expansion is decreased for PDPP[T]$^-$ compared to swelling during water vapor studies. This nonintuitive difference is caused by the presence of electrolyte ions here. Dynamic exchange of TMA$^+$ with K$^+$ increases intermolecular interaction of the polymer chains and, in turn, decreases the lamellar expansion. However, as observable in Figure S31, this is still associated with a significant decrease in scattering intensity and, in turn, overall crystallinity. As observed above, PDPP[Tz]$^-$ does not result in working devices; therefore, this lack of data is not consequential.

The changes in 100 and 010 peaks from the dry state to passive swelling and under active swelling at applied biases of −800 and +800 V are compared. Two examples (PDPP[T]$^+$ and PDPP[Tz]$^+$, chosen here based on the pronounced peak shift and high scattering intensity) for the structural variation in operando are given in Figure 7, with the complete set of data for all of the polymers in Figure S31.

Upon comparison of the scattering data collected in vacuo and during water contact, a significant shift of the 100 peaks of the materials toward lower Q-values is observable (Figure 7a,b, region I). Drastic changes in 100 scattering signals were observed for the cationic CPEs, PDPP[T]$^+$ and PDPP[Tz]$^+$, whereas the changes in 010 peaks for all of the polymers are less pronounced. This variation is caused by water uptake into the interlamellar crystallite space, identical to the kinetic studies conducted with water vapor as discussed previously. Additional application of gating bias leads to further lamellar expansion and contraction of the π−π distance (cf. Figure S31). While this behavior may not be fully intuitive, the observations agree with previous findings.[35]

The active swelling process (i.e., swelling under applied bias) was further examined by applying both oxidative potentials for

https://doi.org/10.1021/acsami.5c19784
ACS Appl. Mater. Interfaces 2026, 18, 8493−8506

donor materials and reductive potentials for acceptor materials, as well as their respective inverse biases (Figure 7a,b, region II). As confirmed by the SEC, these inverse potentials do not induce electrochemical doping in the unipolar polymers. However, an expansion of the interlamellar spacing is still observed across all polymers (Figure S31), particularly notable in cationic polyelectrolytes PDPP[T]$^+$ and PDPP[Tz]$^+$. This expansion occurs without significantly altering the $\pi-\pi$ distance and is attributed to the formation of an electric field between the substrate and gating electrodes. The field promotes additional ion diffusion into the interlamellar polymer space, even under nonreactive conditions. Upon doping, hydrated ions further penetrate the film to compensate charges on the polymer backbone, leading to a more pronounced increase in interlamellar spacing under reactive redox conditions (Figure 7a,b, region III). By distinguishing these different contributions to active swelling, we can, for the first time, split the active swelling regime into distinct regions, I, II, and III, based on the underlying swelling mechanisms. Assuming that cations and anions behave symmetrically, the relative changes in spacing can be categorized into three regions and quantified, as shown in Figure 7c.

The correlation between backbone charge carriers and side-chain charges and the behavior in the OECTs is affected by the different swelling behavior of the polymers. PDPP[T]$^+$ shows a much higher extent of 100 expansion, compared to its anionic counterpart. Likewise, PDPP[Tz]$^-$ swells to an extent that proper analysis is not even possible, whereas PDPP[Tz]$^+$ exhibits more moderate changes in the lamellar spacing. However, when the changes in 010 scattering peaks are considered, a stronger contraction is observable for PDPP[T]$^-$ than for PDPP[T]$^+$. Both moderate lamellar expansion and more pronounced $\pi-\pi$ contraction are beneficial for efficient charge transport. While this may not be the sole reason for the drastic changes in device parameters, it is safe to assume that it is a significant factor.

CONCLUSION

A series of PDPP-based donor and acceptor polymers and polyelectrolytes was synthesized in order to investigate the correlation between main-chain charge carriers and side-chain ionic charges in the OMIEC materials for the OECT applications. By modification of the DPP flanking units, the majority charge carrier in the OECTs was tuned, based on the difference between thiazole- and thiophene-flanked DPPs. Side-chain charges were introduced via polymer-analogous substitution reactions on the comonomer moiety. GIWAXS measurements revealed morphology changes both in vacuo and during passive swelling. In agreement with the water affinity suggested by TGA, anionic polyelectrolytes exhibited a significant increase in the lamellar spacing when exposed to water vapor. This effect was less pronounced for cationic CPEs and minimal in neutral materials.

The distinct influence of the immobilized side-chain ions on electron and hole transport was evident in operando measurements in aqueous electrolytes. SEC and OECT experiments showed a decrease in redox onset for donor materials when anionic groups were attached, whereas cationic groups led to an increase. Interestingly, the opposite trend was observed for electron-transporting materials: cationic groups on the side chain enabled reduction at lower voltages compared with neutral and anionic groups. This behavior was further supported by structural evolution observed during operando GIWAXS measurements.

The impact of these drastic changes in electrochemical properties translated into the OECT characteristics. For donor materials, anionic side chains led to earlier oxidation, large drain current, and higher transconductance compared to neutral and cationic analogs, with performance metrics of V_{th} = −445 mV and μC^* = 9.0 F cm^{-1} V^{-1} s^{-1}. In contrast, for acceptor materials, anionic side chains failed to produce functional OECTs, whereas cationic CPEs demonstrated favorable performance, with V_{th} = 455 mV and μC^* = 5.2 F cm^{-1} V^{-1} s^{-1}. From these results, an empirical design principle emerges: opposite charges between the OMIEC side-chain ions and the main-chain charge carrier (in operando) are beneficial for the development of OECT applications. This may be due to a fast and facile charge self-compensation in the oxidized state via side-chain anions (at applied gate bias) in an anionic donor CPE PDPP[Tz]$^-$ and in the reduced state via side-chain cations in a cationic acceptor CPE PDPP[Tz]$^+$. This principle, however, requires further validation with alternative polymer backbones beyond PDPP and polythiophene. Future studies could refine this approach by exploring variations in the side-chain charge density.

EXPERIMENTAL SECTION

Materials

Reactions sensitive to humidity and oxygen were conducted under a protective argon atmosphere in Schlenk apparatuses, which were previously flame-dried under high vacuum. Anhydrous solvents were purchased from Sigma-Aldrich/Acros Organics in sealed bottles with molecular sieves and used as received. Chloroform was purchased from Sigma-Aldrich. All other solvents, for example, for workups or Soxhlet extractions, were freshly distilled in-house.

$CDCl_3$ (99.95%) was supplied by Deutero, Germany. Potassium carbonate (99.5%) was purchased from Sigma-Aldrich and dried at 500 °C under high vacuum before synthesis. Reagents were used as received from commercial sources if not stated otherwise. Reactions under microwave irradiation were carried out using a Biotage Initiator + synthesis microwave. NMR spectra were recorded on a Bruker Avance spectrometer (300 MHz) at room temperature.

The detailed synthetic procedures are included in the SI.

OFET Device Characterization and Fabrication. Bottom-gate/bottom-contact organic field-effect transistors (OFET Gen4) were purchased from Fraunhofer IPMS. N-doped silicon (doping at the surface ∼3 × 10^{17} cm^{-3}) was used as the surface and gate electrode. The dielectric consists of a 230 ± 10 nm layer of silicon oxide. Each substrate consisted of 16 devices with a constant channel width W of 10 mm and varying channel lengths L of 2.5−20 μm. The source and drain electrodes were a 30 nm thick gold layer on a 10 nm ITO adhesion layer. The devices were prepared by cleaning in acetone and subsequently in isopropanol in an ultrasonic bath for 15 min, followed by 15 min treatment in an ozone oven at 50 °C. The SiO_2 surface was passivated by a 2 h treatment in hexamethylenedisilazane (HMDS) vapor at 100 °C. The devices were rinsed with isopropanol and dried with nitrogen. Thin polymer films were spun cast from 5 mg·mL^{-1} solutions ($CHCl_3$ for neutral polymers, MeOH for anionic CPEs, and MeOH: $CHCl_3$ = 1:1 (v:v) for cationic CPEs) at a spinning speed of 3000 rpm under ambient conditions. All devices were stored and measured under a nitrogen atmosphere. The $I-V$ characteristics were measured by using an Agilent B1500 semiconductor parameter analyzer. Using eq 1, the charge carrier mobility μ was calculated from the slope of the $(I_D)^{0.5} - V_G$ plots, where V_t is the threshold voltage and C_i is the SiO_2 insulator capacitance.

$$I_D = \frac{W}{2L} C_i \mu (V_G - V_t)^2 \quad (1)$$

https://doi.org/10.1021/acsami.5c19784
ACS Appl. Mater. Interfaces 2026, 18, 8493−8506

Grazing-Incidence Small-Angle X-ray Scattering (GIWAXS), Ex-Situ

GIWAXS on neat films coated with silicon substrates was performed in a vacuum at RT on the SAXS/WAXS beamline with a photon energy of 15 keV.[36] The setup included a Pilatus 2 M detector, which was used to record the 2D scattering patterns. Each image consists of three superimposed acquisitions with different relative sample−detector positions at identical distances to obtain the gapless scattering data. A silver behenate reference standard was used to calibrate the sample-to-detector distance. The sample and detector were placed in a vacuum chamber to reduce the air scatter. Measurements were taken as a function of the angle of incidence, with data shown at an angle of incidence near the critical angle that maximized scattering intensity from the sample. Data evaluation and wedge correction were conducted using a modified Nika software package in IgorPro 8.38.1. *Q*-profiles are cake cuts covering an azimuthal angle of 75−105° for the cuts in the vertical direction and 0−15° as well as 165−180° for the cuts in the horizontal direction. Annealed samples were subjected to thermal treatment under an air atmosphere.

Grazing-Incidence Small-Angle X-ray Scattering (GIWAXS), In-Situ

For in situ measurements, the ex-situ measurement setup was modified: The sample stage was placed in air, and the X-ray source and detector were sealed with mica windows. For time-resolved measurements, single images were taken for higher time resolution, as opposed to the images superimposed during static measurements. The GIWAXS acquisition time was 0.5 s, during which the sample stage was translated horizontally to minimize beam damage. The setup for in situ measurements without applied bias is depicted in Figure S19, for operando measurements with applied bias in Figure S30.

^{1}H NMR Spectroscopy

^{1}H NMR spectra (with 64−2048 scans) of small molecules were recorded using a Bruker Avance 250 spectrometer at a working frequency of 300 MHz. Chemical shifts are given in ppm, and coupling constants (J) in Hertz (Hz). The spectra were referenced to the residual solvent peak of CDCl3 (δ = 7.26 ppm).

^{1}H NMR spectra (256 scans) of polymers and ^{13}C NMR spectra (1024 scans) were recorded on a Bruker AVIII HD 500 MHz NMR spectrometer equipped with a 5 mm *z*-gradient broadband 1H/19F−X multinuclear (BBFO) SMART probe using the software TopSpin (version 3, Bruker BioSpin).

Atomic Force Microscopy (AFM)

AFM was measured using a Bruker Dimension Icon Atomic Force Microscope using PeakForce QNM mode with a ScanAsyst-Air probe in an argon-filled glovebox. Samples were spin-cast from 10 mg mL^{-1} solutions in appropriate solvents or solvent mixtures (anionic CPEs: methanol, cationic CPEs: methanol/chloroform = 1/1, neutral polymers: chloroform) onto silicon substrates.

Thermogravimetric Analysis (TGA)

TGA thermograms were recorded using a Mettler Toledo TGA/DSC 3+. Measurements were conducted under N_2 atmosphere between 30 and 700 °C at a heating rate of 10 K min^{-1}. Specimens (between 5 and 7 mg) were filled into Al_2O_3 crucibles (volume of 70 μL).

Gel Permeation Chromatography (GPC)

GPC measurement was performed on an instrument having an SDV linear XL gel column (particle size = 5 μm) with a separation range from 100 to 30,00,000 Da (PSS, Mainz, Germany) together with a refractive index detector (1200 Series, Agilent Technologies). $CHCl_3$ (HPLC grade) was used as the solvent (for dissolving polymer and as an eluting solvent) with a flow rate of 0.5 mL min^{-1} at room temperature. As an internal standard, toluene (HPLC grade) was used. The calibration was done with narrowly distributed polystyrene (PS) homopolymers (PSS calibration kit). An injection volume of 20 μL was used for the measurements. The sample was dissolved in $CHCl_3$ and filtered through a 0.22 μm PTFE filter before analysis.

Spectroelectrochemistry (SEC)

SEC measurements were performed using a Jasco V-670 spectrophotometer combined with a Gamry Interface 1010 Potentiostat/Galvanostat. Thin polymer films were spin-cast onto ITO (1000 s^{-1}, 60 s, 40 μL) from 10 g L^{-1} solutions ($CHCl_3$ for neutral polymers, MeOH for anionic CPEs, and MeOH:$CHCl_3$ = 1:1 (v:v) for cationic CPEs). The films were measured via a three-electrode setup comprising a Pt-counter electrode and a Ag/AgCl reference electrode. The polymer film on ITO was placed in a measurement cell filled with 0.1 M aq KCl solution. The measurements were performed by biasing the film under potentiostatic conditions in 100 mV steps. UV−vis-NIR curves were recorded (1550−300 nm) after the working electrode current reached a steady state (10 s).

Cyclic Voltammetry (*C*−*V*)

Cyclic voltammetry was performed using a Gamry Interface 1010 Potentiostat/Galvanostat, with a three-electrode setup. Polymer films were measured in water with KCl (0.1 M) as the electrolyte. Thin films were spin-cast (3000 rpm, 60 s, 40 μL) onto ITO from 10 g L^{-1} solution ($CHCl_3$ for neutral polymers, MeOH for anionic CPEs, and MeOH:$CHCl_3$ = 1:1 (v:v) for cationic CPEs). The samples were then measured using a Pt-counter electrode and a standard Ag/AgCl reference electrode for the measurement. All electrolytes were degassed with an argon flow for 10 min before each measurement. Scans were recorded at a scan rate of 50 or 100 mV s^{-1}, with a step size of 2 mV.

OECT-Device Fabrication and Characterization

Microstructured substrates for OECTs were developed together with, and purchased from, Fraunhofer Institute for Electronic Nano Systems, Chemnitz, with an architecture consisting of a silicon oxide wafer, 10 nm chromium adhesion layer, 100 nm patterned gold electrodes, and two parylene C layers with a thickness of 2 μm each. The channel widths were varied between 5 and 15 μm. The polymer solutions were spin-coated with a concentration of 10 g L^{-1} at 1000 rpm, yielding film thicknesses of around 90 nm. The film thicknesses were measured by using a DEKTAK 150 stylus profilometer. The Ag/AgCl gate electrode was activated before measurement by dipping it into a diluted bleach solution (e.g., Domestos) for 15 min, followed by thorough rinsing with deionized water. A clean custom-made PDMS holder was placed onto the substrate, its cavity was filled with the electrolyte solution, the gate electrode was placed in the electrolyte droplet (100 mM KCl (aq)), and the source and drain electrodes were contacted. Transistor characteristics were measured using a Tektronix Keithley 2636B source meter and Keithley KickStart Software. The transconductance g_m was obtained by numerical derivation of the drain current with respect to the gate voltage. For obtaining the OECT characteristics, the following OECT equation was used:

$$dI/dV = g_m = Wd/L\mu C^*(V_{th} - V_g) \quad (2)$$

From the above, the figure of merit (μC^*) was extracted by plotting the transconductance g_m vs $WdL{-}1(V_g{-}V_{th})$ and fitting the linear regime. The slope of the linear fit equals where g_m, transconductance; W, channel width, d, film thickness; L, channel length; μ, (OECT) charge carrier mobility; C^*, volumetric capacitance; V_{th}, threshold voltage; V_g, gate voltage. The threshold voltage was determined by the x-axis intercept of the linear regime of $I_d^{0.5}$ versus V_g.

Electrochemical Impedance Spectroscopy (EIS)

EIS measurements were carried out using a Metrohm Germany PGSTAT 204 analyzer module and a NOVA 2.1 software package for analysis. For the measurement, a butylene rubber gasket with a circular aperture of 1 cm diameter was placed on top of the OECT substrates and mechanically pressed onto the substrate with a UHMWPE microcell of 2 mL capacity. The cavity was filled with 1.5 mL of aqueous 0.1 M KCl solution and allowed to settle for 5 min. The underlying planar electrode was used as the working electrode

https://doi.org/10.1021/acsami.5c19784
ACS Appl. Mater. Interfaces 2026, 18, 8493−8506

and the sense line of the potentiostat. An aqueous Ag/AgCl reference electrode and platinum wire counter electrode were dipped into the electrolyte solution, completing the three-electrode setup. The impedance was recorded up to ± 0.6 V versus Ag/AgCl (aq) in a frequency range of 1 to 100 kHz in 17 discrete potential steps with an equilibration time of 5 s between each step. The system was excited with 1 mV_{RMS} and measured with a resolution of 10 frequency steps per decade.

■ ASSOCIATED CONTENT

Supporting Information

The Supporting Information is available free of charge at https://pubs.acs.org/doi/10.1021/acsami.5c19784.

Detailed monomer and polymer synthesis, OECT data for cationic polythiophene polyelectrolytes, GPC, TGA, UV−vis, OFET, detailed GIWAXS data: dry state, in situ setup for vapor swelling and rolling drop method, OECT transfer curves, and μC^* plots (PDF)

■ AUTHOR INFORMATION

Corresponding Author

Andreas W. Erhardt − *Applied Functional Polymers, University of Bayreuth, Bayreuth 95447, Germany; Department of Materials Science and Engineering, Monash University, Clayton, Victoria 3800, Australia;* Present Address: A.W.E.: Oxford University, Department of Chemistry, Chemistry Research Laboratory, Oxford OX1 3TA, United Kingdom; orcid.org/0009-0006-9349-6632; Email: andreas.erhardt@chem.ox.ac.uk

Authors

Julian Hungenberg − *Applied Functional Polymers, University of Bayreuth, Bayreuth 95447, Germany*

Linus Hager − *Applied Functional Polymers, University of Bayreuth, Bayreuth 95447, Germany*

Florian Meichsner − *Applied Functional Polymers, University of Bayreuth, Bayreuth 95447, Germany*

Meike Kuhn − *Department of Materials Science and Engineering, Monash University, Clayton, Victoria 3800, Australia; Dynamics and Structure Formation, Herzig Group University of Bayreuth, Bayreuth 95447, Germany;* orcid.org/0000-0002-3163-0254

Wen Liang Tan − *Department of Materials Science and Engineering, Monash University, Clayton, Victoria 3800, Australia*

Elena Chulanova − *Department of Chemistry, Chemistry Research Laboratory, Oxford University, Oxford OX1 3TA, U.K.*

Nigel Kirby − *Australian Synchrotron, ANSTO, Clayton, Victoria 3168, Australia*

Mukundan Thelakkat − *Applied Functional Polymers, University of Bayreuth, Bayreuth 95447, Germany; Bavarian Polymer Institute (BPI) University of Bayreuth, Bayreuth 95447, Germany;* orcid.org/0000-0001-8675-1398

Christopher R. McNeill − *Department of Materials Science and Engineering, Monash University, Clayton, Victoria 3800, Australia;* orcid.org/0000-0001-5221-878X

Complete contact information is available at: https://pubs.acs.org/10.1021/acsami.5c19784

Author Contributions

This manuscript was written through contributions of all authors. All authors have given approval to the final version of the manuscript.

Notes

The authors declare no competing financial interest.

■ ACKNOWLEDGMENTS

A.W.E., J.H., and M.T. acknowledge financial support from Deutsche Forschungsgemeinschaft (DFG) (677116, Th 807/12-1), and the Bavarian State Ministry for Science and Art (SolTech). A.W.E., J.H., M.K., and M.T. acknowledge financial support from the International Research Training Group (IRTG) Optical excitations in organic and inorganic semiconductors (OPTEXC, GRK 2817/1). This research was undertaken on the SAXS/WAXS beamline at the Australian Synchrotron, part of ANSTO.[36] A.W.E. gratefully acknowledges Doan Vu, Simon Biberger, Paul Chantler, and Subhalakshmi Kumar for assistance during GIWAXS measurements. The authors thank Rika Schneider for GPC, as well as Adrian Hochgesang for EIS measurements and the determination of C*. This work was also supported by a fellowship of the German Academic Exchange Service (DAAD) for A.W.E. and M.K.

■ REFERENCES

(1) Simon, D. T.; Gabrielsson, E. O.; Tybrandt, K.; Berggren, M. Organic Bioelectronics: Bridging the Signaling Gap between Biology and Technology. *Chem. Rev.* **2016**, *116* (21), 13009−13041.

(2) Inal, S.; Rivnay, J.; Suiu, A.-O.; Malliaras, G. G.; McCulloch, I. Conjugated Polymers in Bioelectronics. *Acc. Chem. Res.* **2018**, *51* (6), 1368−1376.

(3) Harikesh, P. C.; Yang, C.-Y.; Tu, D.; Gerasimov, J. Y.; Dar, A. M.; Armada-Moreira, A.; Massetti, M.; Kroon, R.; Bliman, D.; Olsson, R.; Stavrinidou, E.; Berggren, M.; Fabiano, S. Organic Electrochemical Neurons and Synapses with Ion Mediated Spiking. *Nat. Commun.* **2022**, *13* (1), No. 901.

(4) Tan, S. T. M.; Keene, S.; Giovannitti, A.; Melianas, A.; Moser, M.; McCulloch, I.; Salleo, A. Operation Mechanism of Organic Electrochemical Transistors as Redox Chemical Transducers. *J. Mater. Chem. C* **2021**, *9* (36), 12148−12158.

(5) Ohayon, D.; Druet, V.; Inal, S. A Guide for the Characterization of Organic Electrochemical Transistors and Channel Materials. *Chem. Soc. Rev.* **2023**, *52* (3), 1001−1023.

(6) Flagg, L. Q.; Bischak, C. G.; Onorato, J. W.; Rashid, R. B.; Luscombe, C. K.; Ginger, D. S. Polymer Crystallinity Controls Water Uptake in Glycol Side-Chain Polymer Organic Electrochemical Transistors. *J. Am. Chem. Soc.* **2019**, *141* (10), 4345−4354.

(7) Schmode, P.; Savva, A.; Kahl, R.; Ohayon, D.; Meichsner, F.; Dolynchuk, O.; Thurn-Albrecht, T.; Inal, S.; Thelakkat, M. The Key Role of Side Chain Linkage in Structure Formation and Mixed Conduction of Ethylene Glycol Substituted Polythiophenes. *ACS Appl. Mater. Interfaces* **2020**, *12* (11), 13029−13039.

(8) Giovannitti, A.; Nielsen, C. B.; Sbircea, D.-T.; Inal, S.; Donahue, M.; Niazi, M. R.; Hanifi, D. A.; Amassian, A.; Malliaras, G. G.; Rivnay, J.; McCulloch, I. N-Type Organic Electrochemical Transistors with Stability in Water. *Nat. Commun.* **2016**, *7* (1), No. 13066.

(9) Krauss, G.; Meichsner, F.; Hochgesang, A.; Mohanraj, J.; Salehi, S.; Schmode, P.; Thelakkat, M. Polydiketopyrrolopyrroles Carrying Ethylene Glycol Substituents as Efficient Mixed Ion-Electron Conductors for Biocompatible Organic Electrochemical Transistors. *Adv. Funct. Mater.* **2021**, *31* (20), No. 2010048.

(10) Erhardt, A.; Hochgesang, A.; McNeill, C. R.; Thelakkat, M. A Competitive n-Type OECT Material via Copolymerization of

Electron Deficient Building Blocks. *Adv. Electron. Mater.* **2023**, *9* (7), No. 2300026.
(11) Inal, S.; Rivnay, J.; Leleux, P.; Ferro, M.; Ramuz, M.; Brendel, J. C.; Schmidt, M. M.; Thelakkat, M.; Malliaras, G. G. A High Transconductance Accumulation Mode Electrochemical Transistor. *Adv. Mater.* **2014**, *26* (44), 7450−7455.
(12) Hungenberg, J.; Hochgesang, A.; Meichsner, F.; Thelakkat, M. Self-Doped Mixed Ionic-Electronic Conductors to Tune the Threshold Voltage and the Mode of Operation in Organic Electrochemical Transistors. *Adv. Funct. Mater.* **2024**, *34* (44), No. 2407067.
(13) Brendel, J. C.; Schmidt, M. M.; Hagen, G.; Moos, R.; Thelakkat, M. Controlled Synthesis of Water-Soluble Conjugated Polyelectrolytes Leading to Excellent Hole Transport Mobility. *Chem. Mater.* **2014**, *26* (6), 1992−1998.
(14) Kukhta, N. A.; Marks, A.; Luscombe, C. K. Molecular Design Strategies toward Improvement of Charge Injection and Ionic Conduction in Organic Mixed Ionic−Electronic Conductors for Organic Electrochemical Transistors. *Chem. Rev.* **2022**, *122* (4), 4325−4355.
(15) Carreon, A. C.; Santos, W. L.; Matson, J. B.; So, R. C. Cationic Polythiophenes as Responsive DNA-Binding Polymers. *Polym. Chem.* **2014**, *5* (2), 314−317.
(16) Lohwasser, R. H.; Thelakkat, M. Toward Perfect Control of End Groups and Polydispersity in Poly(3-Hexylthiophene) via Catalyst Transfer Polymerization. *Macromolecules* **2011**, *44* (9), 3388−3397.
(17) Lohwasser, R. H.; Thelakkat, M. Synthesis of Amphiphilic Rod−Coil P3HT- *b* -P4VP Carrying a Long Conjugated Block Using NMRP and Click Chemistry. *Macromolecules* **2012**, *45* (7), 3070−3077.
(18) Schmode, P.; Ohayon, D.; Reichstein, P. M.; Savva, A.; Inal, S.; Thelakkat, M. High-Performance Organic Electrochemical Transistors Based on Conjugated Polyelectrolyte Copolymers. *Chem. Mater.* **2019**, *31* (14), 5286−5295.
(19) Rubio-Magnieto, J.; Azene, E. G.; Knoops, J.; Knippenberg, S.; Delcourt, C.; Thomas, A.; Richeter, S.; Mehdi, A.; Dubois, P.; Lazzaroni, R.; Beljonne, D.; Clément, S.; Surin, M. Self-Assembly and Hybridization Mechanisms of DNA with Cationic Polythiophene. *Soft Matter* **2015**, *11* (32), 6460−6471.
(20) Hager, Linus. Conjugated Polyelectrolyte Multilayers vs. Conjugated Polyelectrolytes: Swelling Behaviour and OECT Performance, Master Thesis; University of Bayreuth: Bayreuth, 2021.
(21) Lukkari, J.; Salomäki, M.; Ääritalo, T.; Loikas, K.; Laiho, T.; Kankare, J. Preparation of Multilayers Containing Conjugated Thiophene-Based Polyelectrolytes. Layer-by-Layer Assembly and Viscoelastic Properties. *Langmuir* **2002**, *18* (22), 8496−8502.
(22) Reinold, P. *From Polythiophenes to Functional Materials: Development of Complex Architectures through Polymer Analogous Modifications, Universität Stuttgart*, 2018 http://elib.uni-stuttgart.de/handle/11682/10162 (accessed Oct 15, 2024).
(23) Stegerer, D.; Liu, T.; Xiong, M.; Wu, H.-Y.; Kang, M. G.; Woo, H. Y.; Fabiano, S.; Sommer, M. Molar Mass Improves the Performance of N-Type Organic Electrochemical Transistors. *Chem. Mater.* **2025**, *37* (14), 5226−5233.
(24) Carsten, B.; Szarko, J. M.; Lu, L.; Son, H. J.; He, F.; Botros, Y. Y.; Chen, L. X.; Yu, L. Mediating Solar Cell Performance by Controlling the Internal Dipole Change in Organic Photovoltaic Polymers. *Macromolecules* **2012**, *45* (16), 6390−6395.
(25) Mueller, C. J.; Gann, E.; Singh, C. R.; Thelakkat, M.; McNeill, C. R. Control of Molecular Orientation in Polydiketopyrrolopyrrole Copolymers via Diffusive Noncovalent Interactions. *Chem. Mater.* **2016**, *28* (19), 7088−7097.
(26) Erhardt, A.; Hungenberg, J.; Chantler, P.; Kuhn, M.; Huynh, T. T.; Hochgesang, A.; Goel, M.; Müller, C. J.; Roychoudhury, S.; Thomsen, L.; Medhekar, N. V.; Herzig, E. M.; Prendergast, D.; Thelakkat, M.; McNeill, C. R. Design Principles of Diketopyrrolopyrrole-Thienopyrrolodione Acceptor$_1$ − Acceptor$_2$ Copolymers. *Adv. Funct. Mater.* **2024**, *34* (32), No. 2314696.
(27) Mauerer, T.; Hungenberg, J.; Thelakkat, M.; Marschall, R. Influence of Poly(Diketopyrrolopyrrole) Chain Length and Chemical Structure on Photocatalytic Hydrogen Evolution in Composites With TiO_2. *J. Polym. Sci.* **2025**, *63*, 4684−4697.
(28) Hong, H. N.; Kim, H. J.; Kim, A.; Choi, S.; Kim, Y. U.; Cho, M. J.; Choi, D. H. Tunable Intrinsic Semiconducting Properties of Diketopyrrolopyrrole-Based Copolymers with Electron Donating Thiophene and Electron Accepting Thiazole Moieties. *Synth. Met.* **2018**, *236*, 1−7.
(29) Dolynchuk, O.; Kahl, R. T.; Meichsner, F.; Much, A. J.; Pechevystyi, A.; Averkova, A.; Erhardt, A.; Thelakkat, M.; Thurn-Albrecht, T. Controlling Crystal Orientation in Films of Conjugated Polymers by Tuning the Surface Energy. *Macromolecules* **2024**, *57* (21), 10399−10409.
(30) Schneider, S.; Gotthardt, J. M.; Steuer, L.; Leingang, S.; Himmel, H.-J.; Zaumseil, J. Improving Electron Injection and Transport in Polymer Field-Effect Transistors with Guanidino-Functionalized Aromatic n-Dopants. *J. Mater. Chem. C* **2021**, *9* (23), 7485−7493.
(31) Vu, D.; Tang, L.; Thomsen, L.; Jevric, M.; Andersson, M. R.; McNeill, C. R. Formation and Charge Transport Properties of P(NDI2OD-T2) Thin Films with End-on Oriented Form III Crystallites. *Chem. Mater.* **2023**, *35* (14), 5550−5561.
(32) Huang, L.; Wang, Z.; Chen, J.; Wang, B.; Chen, Y.; Huang, W.; Chi, L.; Marks, T. J.; Facchetti, A. Porous Semiconducting Polymers Enable High-Performance Electrochemical Transistors. *Adv. Mater.* **2021**, *33* (14), No. 2007041.
(33) Paleti, S. H. K.; Haraguchi, S.; Cao, Z.; Craighero, M.; Kimpel, J.; Zeng, Z.; Sowinski, P.; Zhu, D.; Pons I Tarrés, J.; Kim, Y.; Li, Q.; Huang, J.; Kalaboukhov, A.; Mihiretie, B.; Fabiano, S.; Gu, X.; Müller, C. Benchmarking the Elastic Modulus of Conjugated Polymers with Nanoindentation. *Macromolecules* **2025**, *58* (7), 3578−3588.
(34) Savva, A.; Hallani, R.; Cendra, C.; Surgailis, J.; Hidalgo, T. C.; Wustoni, S.; Sheelamanthula, R.; Chen, X.; Kirkus, M.; Giovannitti, A.; Salleo, A.; McCulloch, I.; Inal, S. Balancing Ionic and Electronic Conduction for High-Performance Organic Electrochemical Transistors. *Adv. Funct. Mater.* **2020**, *30* (11), No. 1907657, DOI: 10.1002/adfm.201907657.
(35) Flagg, L. Q.; Asselta, L. E.; D'Antona, N.; Nicolini, T.; Stingelin, N.; Onorato, J. W.; Luscombe, C. K.; Li, R.; Richter, L. J. In Situ Studies of the Swelling by an Electrolyte in Electrochemical Doping of Ethylene Glycol-Substituted Polythiophene. *ACS Appl. Mater. Interfaces* **2022**, *14* (25), 29052−29060.
(36) Kirby, N. M.; Mudie, S. T.; Hawley, A. M.; Cookson, D. J.; Mertens, H. D. T.; Cowieson, N.; Samardzic-Boban, V. A Low-Background-Intensity Focusing Small-Angle X-Ray Scattering Undulator Beamline. *J. Appl. Crystallogr.* **2013**, *46* (6), 1670−1680.

https://doi.org/10.1021/acsami.5c19784
ACS Appl. Mater. Interfaces 2026, 18, 8493−8506